Rotational transitions in a C_{60} monolayer on the WO_2/W(110) surface

Sergey I. Bozhko,[1,2] Sergey A. Krasnikov,[1] Olaf Lübben,[1] Barry E. Murphy,[1] Kevin Radican,[1] Valery N. Semenov,[2] Han Chun Wu,[1] Brendan Bulfin,[1] and Igor V. Shvets[1,*]

[1]*Centre for Research on Adaptive Nanostructures and Nanodevices, School of Physics, Trinity College Dublin, Dublin 2, Ireland*

[2]*Institute of Solid State Physics, Russian Academy of Sciences, Chernogolovka 142432, Russian Federation*

(Received 24 August 2011; revised manuscript received 6 October 2011; published 3 November 2011)

Variable-temperature scanning tunneling microscopy (STM) is shown to be an effective technique to study two-dimensional phase transitions. Observations show that a monolayer of C_{60} deposited on an ultrathin WO_2 layer grown on the W(110) surface undergoes a structural phase transition at 259 K, similar in temperature to that of bulk C_{60}. In turn, a kinetic transition has been observed at 220 K, which is significantly higher than that of the bulk C_{60} crystal (90 K). This difference is attributed to interactions between the molecular overlayer and the substrate, as well as correlation effects within the C_{60} film. Different types of molecular nanomotion, such as rotation, spinning, and switching between different orientations, have been observed. STM measurements are supported by density functional theory calculations, which provide confirmation of different orientations of C_{60} on the WO_2 thin film.

DOI: 10.1103/PhysRevB.84.195412 PACS number(s): 68.37.Ef, 68.18.Jk, 61.66.Hq, 61.48.−c

I. INTRODUCTION

The study of phase transitions in two-dimensional (2D) systems is an active area of research due to their potential applications, such as improving the performance of liquid crystal opto-electronic devices[1] and high-T_C superconductors,[2,3] and also due to the fundamental physics at play. There are major differences between phase transitions in 2D and 3D systems.[4–7] For example, melting in 3D crystals is always a first-order transition, whereas in 2D systems this is not necessarily the case. Since the discovery of C_{60}, much attention has been paid to the development of C_{60}-based electronic devices and sensors.[8–10] In a close-packed, two-dimensional layer of C_{60} molecules, individual molecules are weakly bonded to their nearest neighbors. If each molecule in such a monolayer could be addressed individually, this could provide the basis for a device with an ultrahigh element density. The properties of such devices are determined by the behavior of both the individual molecules and the C_{60} layer as a whole.

The unique properties of fullerenes and fullerene-based compounds result from the structure and shape of the C_{60} molecule. The symmetry of the molecule and its deviations from a uniform spherical shape give it rotational degrees of freedom, which often determine the physical properties of C_{60} compounds, C_{60}-based clusters, 2D layers, and the 3D crystal. At room temperature, C_{60} molecules arranged in a face-centered cubic lattice (fcc) undergo rapid rotation around their centers of mass. The typical time for a single molecular rotation is in the range of 3 picoseconds.[11] Below 259 K, however, ordering occurs, resulting in a change of space group symmetry from fcc to simple cubic.[12–14] Neutron scattering studies[13,15] have shown that between 90 K and 259 K, C_{60} molecules in the 3D crystal shuffle between two nearly degenerate orientations, which differ in energy by 11 meV. The orientations are separated by an energy barrier of 290 meV.[16,17] There is a glassy transition at 90 K, resulting from a freezing of the molecules' hopping between the two orientations.[18] The relaxation time is estimated to be about 1 day at 90 K.[19,20] The relaxation process around the glassy transition can be fitted by a nonexponential function $\exp\{-(t/\tau)^{\beta}\}$,[18] where $\beta = 0.94$.[20] The deviation of the relaxation dependency from a simple exponential ($\beta = 1$) curve provides evidence for significant interaction between molecules.

The rotational phase transition in an 80 nm, single-crystalline C_{60} film deposited on GaAs(111) has been previously studied by XRD.[21] The results of these measurements reveal an anomaly in the lattice parameter at the phase transition temperature $T_C = 240$ K, 20 K below that of the bulk C_{60} crystal. This difference was attributed to a strain effect in the C_{60} film introduced by the substrate.

Mean-field theory has been used to model the interactions of solid C_{60}, both on the surface of the crystal and in the bulk, and these calculations have been confirmed by experimental results. In solid C_{60}, melting of the orientational order starts from the top layer of the surface. Lu *et al.*[19] and Lamoen and Michel[22] have each modeled the interactions in bulk C_{60} using mean-field techniques and were able to reproduce the experimentally observed crystal symmetries, including the phase transition from a low-temperature simple cubic structure to a disordered face-centered cubic structure at 260 K.

Passerone and Tosatti[23] and Laforge *et al.*[24] later built upon these models to describe the rotational surface disordering phase transition for the (111) surface of solid C_{60}, for which three separate phases are predicted and observed. Below 150 K, the surface has (2×2) symmetry. Three molecules in the surface (2×2) unit cell have only a twofold axis normal to the surface. The fourth, more frustrated molecule has instead its threefold axis normal to the surface. Between 150 K and 230 K, the surface symmetry is still (2×2), but the more frustrated molecule begins to rotate, and above 230 K, all surface molecules are in the disordered state, with (1×1) surface symmetry.

This present work is focused on the link between an individual molecule's transitions between different states and the phase transition of a statistical ensemble of C_{60} molecules forming a single molecular layer. Scanning tunneling microscopy (STM) experiments with molecular orbital resolution were carried out on a C_{60} monolayer formed on the WO_2/W(110) surface in the temperature range between

78 K and 320 K. A rotational phase transition at 259 K and a kinetic glassy transition at 220 K have been observed. We have found a good agreement between the parameters of the observed rotational transitions and those predicted from the properties of individual C_{60} molecules.

II. EXPERIMENTAL

Experiments were performed using a variable-temperature STM from Createc in an ultrahigh-vacuum (UHV) chamber with a base pressure of 4×10^{-11} mbar. The STM tips were fabricated from [001]-oriented $0.3 \times 0.3 \times 10$ mm^3 single-crystalline tungsten bars by electrochemical etching in 2 M NaOH and cleaned in the UHV chamber by Ar^+ ion bombardment.[25] An O-W-O trilayer structure was formed on the W(110) surface by annealing the single-crystalline tungsten sample in oxygen ($P = 10^{-6}$ mbar) for 20 min at 1300 °C, producing oxide rows along the [337] direction.[26] The row width of 2.46 nm and the crystallographic direction of the oxide rows were determined by low-energy electron diffraction (LEED) and confirmed by STM. The WO_2/W(110) surface was covered with monatomic steps and terraces up to 50 nm in width. Oxide rows and monatomic steps were used to calibrate the STM scanner in the subsequent variable temperature experiment. C_{60} (Sigma Aldrich) was deposited onto the oxidized W(110) surface at room temperature using a Knudsen cell. The STM scanning unit was cooled down to 78 K and the deposited film was quenched once it was loaded into the cold STM. During the variable temperature measurements, the whole scanning unit was heated up, initially resulting in a noticeable thermal drift. 15–20 hours after switching on the heater, the temperature was stabilized with an accuracy of 0.1 K, and the drift was reduced to less than 1 Å per minute. All STM images were acquired in a constant current mode ($I_t = 0.1$ nA).

III. RESULTS

A. C_{60} film structure

The self-assembly of C_{60} molecules deposited onto the WO_2/W(110) substrate at room temperature results in the growth of C_{60} islands, one monolayer in height.[27] The island size depends on the coverage, but in general a nearly perfectly completed monolayer could be formed in this way, starting from the inner step edges of the WO_2/W(110) surface. STM images of the C_{60} monolayer acquired at different temperatures are presented in Fig. 1. The molecules form a close-packed layer with a hexagonal structure and one of the close-packed directions of the C_{60} layer coincides with the [001] direction of the W(110) surface.[27] The observed C_{60}-C_{60} distance is equal to 9.5 ± 0.5 Å, which is comparable to the intermolecular distance of 10 Å in bulk C_{60} crystal.[13] The height from the substrate surface to the molecules' centers was 5 Å, as measured by STM of the fullerene film thickness at the edges of the closed C_{60} layer.

B. Temperature dependance

At low temperatures (below 220 K), STM images of individual molecules reveal an orbital structure that is determined by the orientation of the C_{60} molecule [Figs. 1(a) and 1(b)]. The arrangement of the molecular orbitals depends on the cooling regime. When the sample was quenched with a cooling rate of 10 K/min, it formed the orbital structure presented in Fig. 1(a). This structure is characterized by a random orientation of C_{60} molecules forming a glassy, metastable state. No correlations between the individual orientations of neighboring C_{60} molecules have been found. The orbital arrangement realized by slow cooling of the film, at a rate of 100 K/day, from 300 K down to 78 K, is shown in Fig. 1(b). The molecular orbitals of individual C_{60} appear in the STM image of the orbital-correlated state as stripes aligned in one direction [Fig. 1(b)]. Almost all C_{60} molecules in Fig. 1(b) exhibit this striped structure, which indicates that these molecules face the substrate with an h-h bond.[27] Orbital alignments both along and perpendicular to a close-packed direction of the molecular layer have been observed. As the state shown in Fig. 1(b) results from slow cooling, it would suggest that the alignment with the h-h bonds facing the substrate has lower energy than the glassy, metastable state obtained by quenching the sample. In this paper we use common notations for states characterized by different bonds between C_{60} and the surface: h, h-h, p, h-p, and s states. These are discussed in greater detail below, in relation to Figs. 4 and 5.

At a temperature of 78 K, the majority of the molecules retained their orbital structure and they were static for the duration of the experiment (up to several days), regardless of whether they were in the h-h or h-p state. In contrast, at high temperatures ($T > 259$ K), the orbital structure of individual

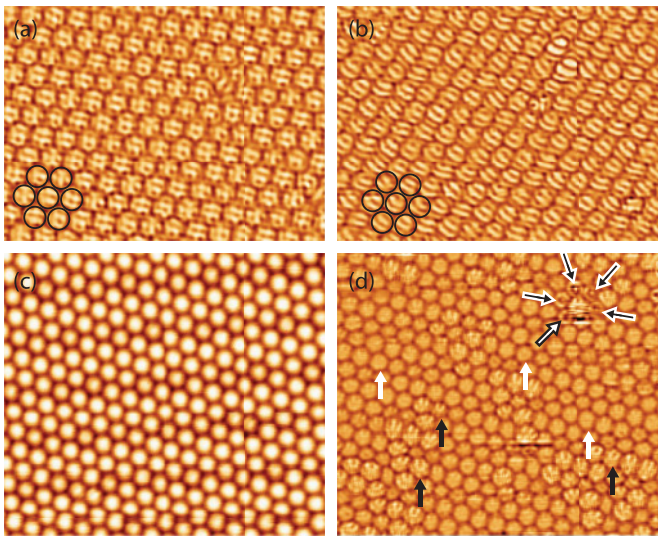

FIG. 1. (Color online) STM images of the C_{60} monolayer at different temperatures. (a) and (b) 12×14 nm^2 STM images acquired at $T = 78$ K. (a) Image of quenched C_{60} film; (b) image of the C_{60} film obtained by slow cooling at a rate of 100 K/day. Highlighted in black in panels (a) and (b) are the outlines of individual molecules. (c) and (d) 19×16 nm^2 STM images of the same C_{60} film acquired at $T = 315$ K and $T = 256$ K, respectively. All molecules in (c) appear as perfect spheres due their fast rotation. Solid black arrows in panel (d) indicate examples of static C_{60} molecules, solid white arrows show molecules with unresolved orbital structure, and black-outlined and white-outlined arrows point to spinning molecules with a dip or a protrusion at the center, respectively (see text).

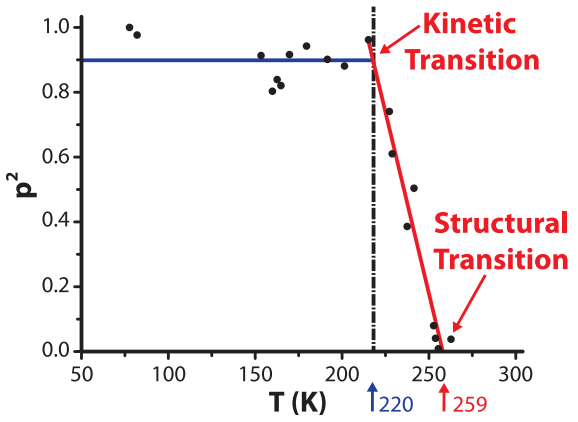

FIG. 2. (Color online) Squared probability of finding a static C_{60} molecule, p^2, versus temperature, T. Blue (220 K) and red (259 K) arrows indicate the temperatures of kinetic and structural rotational transitions, respectively. In the temperature range from 220 K to 259 K, p^2 is fitted by a linear function $p^2 = \alpha(T_C - T)$, where $\alpha = 0.022 \pm 0.002\ \mathrm{K}^{-1}$ and $T_C = 259$ K.

C_{60} molecules is no longer visible in STM images [Fig. 1(c)] due to the molecules' rotation, which is faster than the time resolution of the STM. All C_{60} molecules appear in these STM images as perfect spheres.

At intermediate temperatures (220 K $< T <$ 259 K), both static and rotating molecules appear in the STM images [Fig. 1(d)]. In the temperature range 220 K $< T <$ 259 K the fraction of static molecules rapidly decreases with increasing temperature.

At $T <$ 220 K, almost all molecules exhibit the orbital structure. The few anomalies are likely caused by defects on the surface. Figure 2 shows the temperature dependence of the square of the probability of finding a static C_{60} molecule, p^2, to demonstrate the observed transitions and reveal the order parameter η. According to Landau's theory of phase transitions, the order parameter η is proportional to $(T_C - T)^{1/2}$. At low temperatures ($T <$ 220 K), p^2 is constant with respect to temperature, but does not quite reach unity, since the few molecules close to the defects appearing in the STM images were not included in the number of static molecules. The horizontal blue trend line shown is a fit to the data, with its slope set to 0.

In the temperature range from 220 K to 259 K, p^2 is fitted by a linear function $p^2 = \alpha(T_C - T)$, where $\alpha = 0.022 \pm 0.002\ \mathrm{K}^{-1}$ and $T_C = 259$ K. T_C indicates the temperature of the rotational phase transition. The glassy transition at $T_g = 220$ K is a kinetic transition, at which the molecular switching rate between different states becomes slower than the time scale of the experiment. Below T_g, the C_{60} molecules' nanomotion becomes virtually frozen and orbital-resolved STM images of individual molecules do not change.

C. Molecular transitions between different states

Orbital-resolved STM images of C_{60} present a unique opportunity to study the rotational transition mechanism on the molecular scale. Figure 3 shows a consecutive set of STM

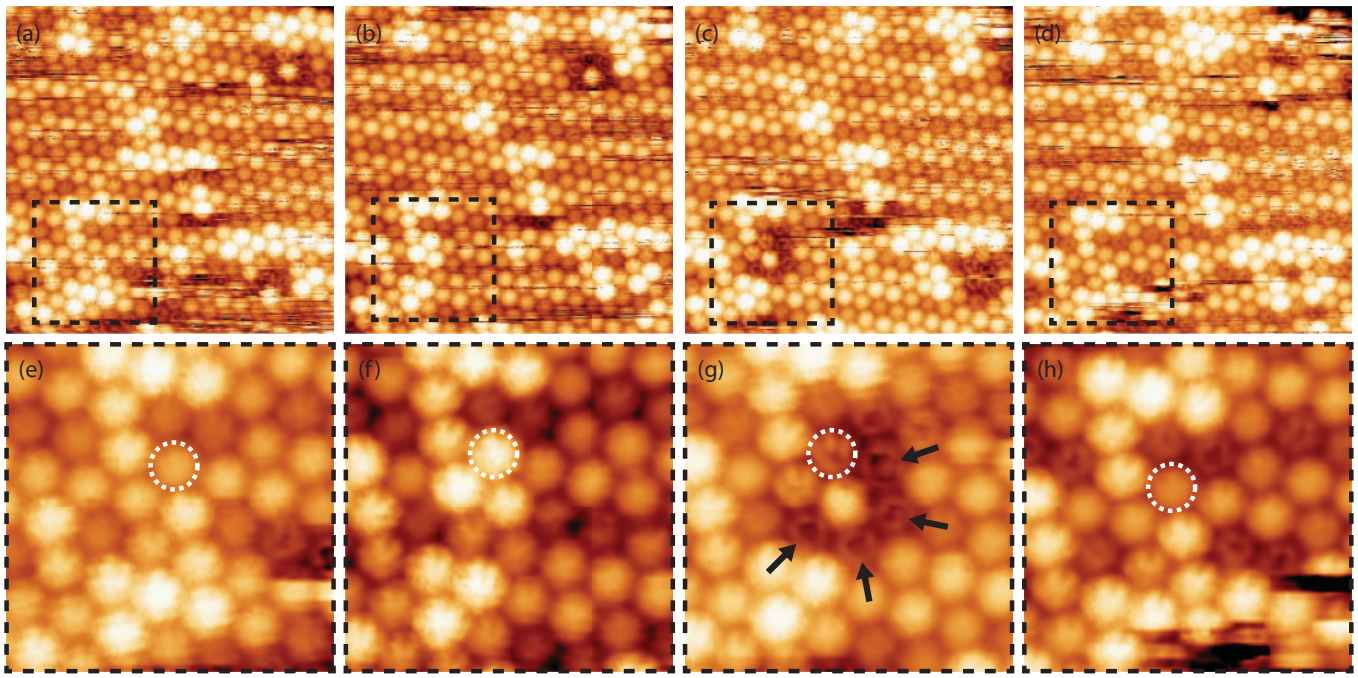

FIG. 3. (Color online) Dynamics of transitions between different molecular states of a C_{60} monolayer at $T = 256$ K. (a)–(d) 19 × 19 nm^2 STM images of the C_{60} film acquired at $V_b = 1.0$ V and $I_t = 0.07$ nA, over a sampling time of 480 sec. Panels (e)–(h) present a zoom of the area marked by the dashed box in panels (a)–(d). The same molecule is indicated by a white circle in (e)–(h) and it can be seen to switch from the medium-conductance state (e) to the high-conductance state (f) and to go from spinning (g) to non-spinning (h). Arrows in panel (g) highlight several molecules that engage in spinning motion, resulting in their ring-shaped appearance. These molecules do not spin in (e) and (f).

images of the C_{60} monolayer measured at $T = 256$ K, in the vicinity of the rotational phase transition, $(T_C - T)/T_C = 0.012$.

The STM images presented in Figs. 3(a)–3(h) indicate how C_{60} molecules can switch between several different states, leading to changes in their appearance. Some molecules switch between a high- and a low-conductance state, observed in STM images as a repetitive switching between a bright and dark appearance. Furthermore, static molecules exhibit an orbital structure,[27] while those with high-magnitude oscillations and molecular rotation appear blurry in STM images.

Panels (e)–(h) show a zoom of the area marked by a dashed box in panels (a)–(d). A single molecule which switches between states in subsequent scans is shown by a dashed circle. The mechanism of a molecule's switching is connected to its rotation, accompanied by charge transfer to or from the molecule, leading to its becoming polarized.[28,29] The molecules can also switch between static (orbitals resolved) and dynamic (orbitals blurred) states.

We also observe molecules that appear in the STM images as a ring shape, or a ring with a protrusion at the center [Fig. 1(c), Figs. 3(e), 3(f), and 3(h)]. Such shapes can be explained by the molecules spinning around their axis perpendicular to the surface. This is shown in detail in Fig. 5. Arrows in Fig. 3(f) indicate several such spinning molecules exhibiting the ring-shape appearance. These molecules do not spin in Fig. 3(e) and Fig. 3(g). From the analysis of an extensive number of STM images we have found that, in many cases, the switching of one molecule into a bright state can trigger the spinning of its nearest neighbors. We also found that spinning molecules tend to occupy positions along the grooves of the WO_2/W(110) substrate, as shown in Fig. 4. This suggests that the energy levels of the C_{60} molecules are affected by the substrate and also that the molecular states can be made more stable or less stable depending on the position of the molecule within the unit cell of the WO_2/W(110) structure. Therefore, in addition to the transition between different orbital states, there are transitions between the static state of the molecule and spinning state (in-plane rotation). Such phenomena are only observed for isolated molecules and molecular clusters in the monolayer, and so are not caused by molecular transfer to the tip or other tip effects, because if that were the case, the tip would affect all molecules being imaged.

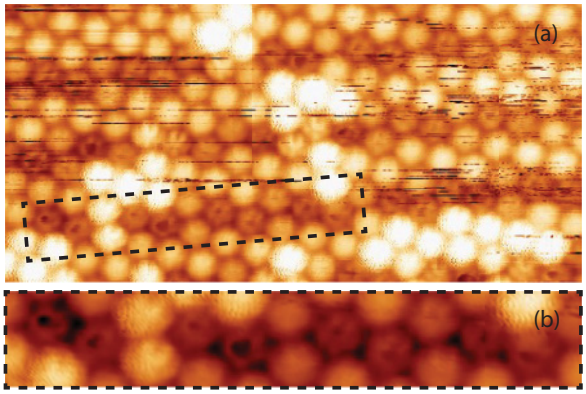

FIG. 4. (Color online) (a) 19×9 nm^2 STM image of the C_{60} film acquired at $V_b = 1.0$ V and $I_t = 0.07$ nA, demonstrating the decoration of the WO_2 rows of the underlying substrate surface by dim C_{60} molecules, $T = 256$ K. (b) Zoom of the area indicated by the dashed box showing a row of spinning molecules.

In order to determine which part of the spinning C_{60} molecules face the WO_2/W(110) surface, we performed density functional theory (DFT) simulations of the partial charge distribution of electron states. Density of states (DOS) calculations were performed using the Vienna *Ab initio* Simulation Package (VASP) program. VASP implements a projected augmented basis set (PAW)[30] and periodic boundary conditions. The electron exchange and correlation was simulated by local density approximation (DFT-LDA) pseudopotentials with a Ceperley-Alder exchange-correlation density functional.[31] A Γ-centered $(2 \times 2 \times 1)$ k-point grid was used for all calculations to sample the Brillouin zone. The applied energy cutoff was 400 eV. The global break condition for the electronic self-consistent loops was set to a total energy change of less than 1×10^{-4} eV.

It has been shown that DFT-LDA has given excellent results for the total energies and band structures of fullerites and other carbon-based structures (graphite, nanotubes).[32–37]

Girifalco and Hodak state that first-principles calculations for graphitic structures can be carried out quite successfully, but they are sensitive to the details of the calculation, and long-range dispersion interactions, such as van der Waals forces, should be included for separation distances greater than 1.15 of the equilibrium separation.[38] However, the separation distance of C_{60}-C_{60} on the WO_2/W(110) surface is 9.5 ± 0.5 Å, which is less than the intermolecular distance of 10 Å in the bulk C_{60} crystal. This strongly suggests that van der Waals interactions can be neglected for the system under investigation in this paper, and that DFT-LDA calculations are sufficient.

In fact, a recent study of graphene sheets on various metal surfaces using the van der Waals density functional (vdW-DF) has shown that vdW-DF incorrectly predicts weak binding for Ni, Co, and Pd, and the substrates had no effect on the band structure of graphene, in direct conflict with experimental low-energy electron diffraction and angle-resolved photoelectron spectroscopy results for the same systems.[39]

To find the optimum surface site of a single C_{60} molecule on one layer of WO_2, several different surface sites were sampled and the total energy of those systems was calculated. The system was found to have the lowest ground-state energy when the C_{60}'s surface-facing C-C bond bridged two surface oxygen atoms, each of which was bonded to a different tungsten atom. This site, herein called site "A," was chosen for all further calculations. To further minimize the energy of the system, different orientations of C_{60} on site A were simulated. For all orientations, the C_{60} molecule was allowed to relax on a constrained layer of WO_2.

DFT calculations of the total free energy reveal that the h-h configuration corresponds to the lowest energy state. The h-p configuration is separated from the lowest energy state by 17 meV, which is comparable to $k_B T$ in our STM experiments. The energy gap between the p and the h-h configurations is about 90 meV. The h and s configurations are the least favorable, being separated in energy from the h-h configuration by 360 meV and 420 meV, respectively. The partial charge density of each of these systems was calculated in the range from E_F to 1 eV, where E_F is the Fermi energy.

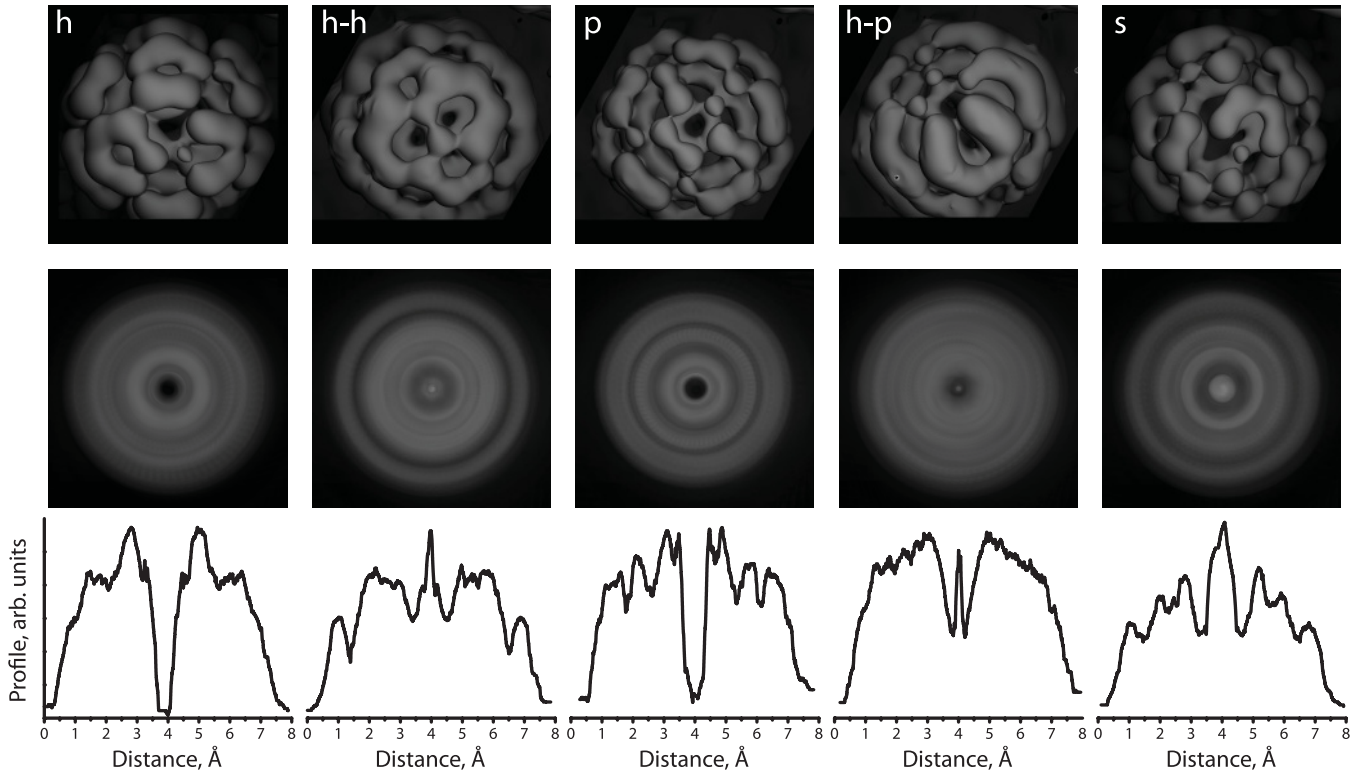

FIG. 5. (Color online) First row: DFT simulations of the partial charge density distribution of electron states of static C_{60} molecules facing the substrate by different parts of the molecule. h and p configurations correspond to the molecule facing the substrate by a hexagon or a pentagon, respectively. In h-h and h-p configurations, C_{60} faces the surface by the C-C bond shared between two hexagons or a hexagon and a pentagon, respectively. Second row: Images obtained by rotating the charge distributions in the top panel in increments of 5°. These represent the weighted electron density of a molecule in a particular configuration with the additional degree of rotation around the axis perpendicular to the substrate. Third row: Cross sections through the rotated charge distribution shown in the second row.

The obtained charge distribution images (Fig. 5, first row) were then processed by rotating them in increments of 5°. The resulting rotated images (Fig. 5, second row) were combined to form a single composite weighted image for each orientation. This represents a molecule spinning too fast for the STM probe to resolve. The charge distribution images for h and p orientations reveal a dip at the center of the molecule while for h-h, h-p, and s orientations, the ring shape of the image is accompanied by a protrusion at the center. Cross-section profiles of these simulated spinning molecules are shown in Fig. 5 for comparison with experiment. STM images of individual spinning molecules were found to have either a ring shape with a dip or dent [Fig. 6(a)] or a protrusion in the center [Fig. 6(c)].

Cross sections of typical STM images of the spinning C_{60} molecules are presented in Fig. 6. Panel (b) corresponds to the dip at the center while (d) corresponds to the protrusion. About 90% of the examined STM images of spinning C_{60} molecules reveal a protrusion at the center of ring-shape images. According to DFT calculations, h-h and h-p orientations are most favorable in energy. Thus, we conclude that most of the spinning molecules face the surface by C-C bonds. The STM image presented in Fig. 6 with a dip at the center of the molecule is most likely due to a spinning molecule faced to the substrate by a pentagon.

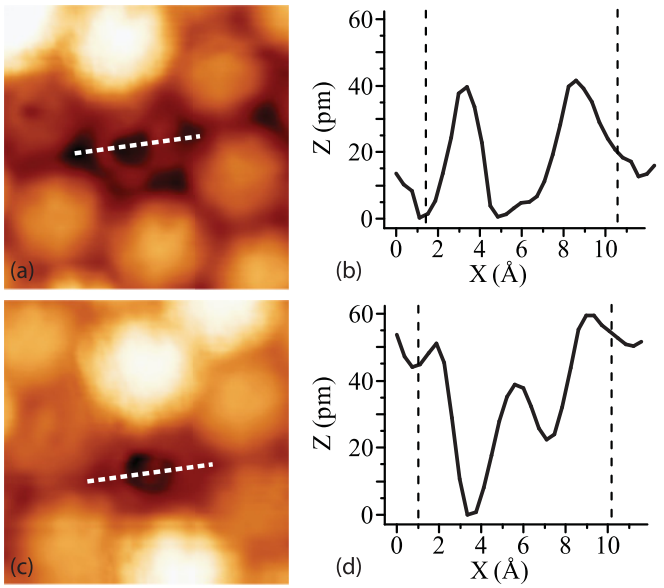

FIG. 6. (Color online) STM images of individual spinning molecules with a dip (a) or a protrusion (c) at the center. Panels (b) and (d) correspond to cross sections along the indicated lines in the STM images of the spinning molecules presented in panels (a) and (c). Dashed lines indicate the boundaries of an individual molecule's cross section.

The peak-to-peak diameter of the holes has been observed to vary between approximately 3–6 Å, and the diameters of the experimental cross sections in Fig. 6 are approximately a factor of 2 larger than those of Fig. 5. This difference, and the distribution of diameters, is attributed to molecular movement on the surface, such as the precession of the spinning axis around the surface normal, for which different precession angles will alter the apparent size of the hole by different amounts. The h and s configurations of the molecules are unlikely to be observed to spin under the present experimental conditions because of the large gap in energy from the ground state. Thus the model suggests that a spinning molecule presents a reasonable explanation for the unusual appearance of the C_{60} molecules observed in the temperature range of 220 K to 259 K.

IV. DISCUSSION

A. Phase transition

In the three-dimensional C_{60} crystal, two transitions are associated with molecular rotation: a first-order transition that takes place at 259 K and a kinetic glassy transition at 90 K.[11–17] Above 259 K, the molecules freely rotate. At lower temperatures, the molecules hop between two orientations separated in energy by about 11 meV. At 90 K, the C_{60} crystal undergoes a glassy transition when the equilibrium relaxation time τ exceeds the laboratory experiment time. τ was estimated to change from 1 second to 1 day between 130 K and 90 K, with a relaxation activation energy W_τ of about 290 meV.[19]

We found that at $T > 259$ K, the C_{60} molecules in the monolayer deposited on the WO_2/W(110) surface freely rotate [Fig. 1(d)], similar to behavior observed in solid C_{60}. In contrast, at lower temperatures ($T < 259$ K) we found significant differences between the monolayer and bulk C_{60}. However, it is surprising that the temperature of the rotational phase transition in the C_{60} monolayer on the WO_2/W(110) surface coincides with that of solid C_{60}.

When very close to the phase transition temperature, fluctuations appear in the form of blinking or spinning molecules. Hence, close to T_C there will be inhomogeneity introduced by these fluctuations but not necessarily large regions of instability, similar to how orientational melting begins at the surface of bulk C_{60}.[24] The amount of these fluctuations decays exponentially away from T_C, and at low temperatures the film looks homogeneous [Fig. 1(b)].

According to mean-field theory,[40] the temperature of a phase transition, $T_C = E/2k_B$, is determined by the total energy of interaction between the molecule and its neighbors. In a C_{60} monolayer, this is determined by the C_{60}'s interaction with its neighboring molecules, the C_{60}-substrate interaction, and the crystal field. The interaction between C_{60} molecules was calculated using several models. Calculations[41,42] reveal that, in the case of C_{60} molecules separated by 1 nm, a distance comparable to the separation between molecules' centers in a monolayer, the dominant contribution is due to the Coulomb interaction between the molecules' respective charge densities. These calculations show that several combinations of the orbital configurations of two adjacent C_{60} molecules are close in energy.

The coordination number of a C_{60} molecule in a monolayer is halved to 6, compared to the 12-fold coordinated fcc bulk lattice. Therefore one could simplistically expect a T_C reduced roughly by a factor of two compared to that of the bulk, if the interaction with the substrate were neglected. Such a reduction is indeed observed on the (111) surface of a C_{60} crystal.[24,43] In contrast, our experiment shows the same value of $T_C = 259$ K for the C_{60} monolayer as that of the bulk, suggesting that an energy contribution on the order of $k_B T_C = 24$ meV originates from the interaction with the substrate.

There are two possible mechanisms for such an interaction: via the crystal field, which has a strong component perpendicular to the substrate due to the breaking of z-translational invariance,[44] or due to the effect of the overlap of the orbitals of the C_{60} molecules and the substrate.

The wave function of the HOMO of a single C_{60} decays out of the molecule over the length scale of a covalent bond (1.4 Å). This is comparable to the distance between the C atoms of an individual C_{60} molecule and the substrate surface atoms, as determined experimentally (approximately 1.5 Å). The importance of the interaction of C_{60} with the substrate is confirmed by the decoration of WO_2/W(110) grooves by spinning molecules [Fig. 4(d)]. This suggests that the energy of the C_{60} is sensitive even to relatively small changes in the environment, such as being brought into closer contact with the substrate due to the WO_2/W(110) coincidence structure.

In the mean-field theory approximation, the order parameter's dependence on the temperature is specified as $p^2 \approx \frac{3(T_C - T)}{T_C} = \alpha(T_C - T)$, where $\alpha = 0.012$ K^{-1}. The experimentally measured value of $\alpha = 0.022 \pm 0.002$ K^{-1} is approximately a factor of two greater than that predicted by theory. One reason for this discrepancy is that correlation effects are ignored by mean-field theory. Examples of such correlation effects that have been observed are presented in Fig. 1(d), where it is shown that static molecules form clusters, and their orientations within the clusters are correlated. This implies that the total energy of a molecule's interaction with its neighbors is also affected by its configuration on the substrate.

B. Kinetic transition

The glassy transition and nonexponential relaxation in solid C_{60} are due to the freezing of weakly correlated orientations of nearest-neighbor molecules.[18] In bulk C_{60}, the molecules can occupy two rotational orientations which are almost equivalent in energy but are separated by a potential barrier, and these orientations are distributed in a random fashion over the sites of an fcc lattice. The relaxation of solid C_{60} is determined by the potential barrier between these two states. All individual molecules in solid C_{60} occupy equivalent positions in the fcc lattice; each molecule relaxes nearly identically in an intrinsically nonexponential manner according to a homogeneous scenario.[45]

This relaxation is characterized by the Kohlrausch-Williams-Watts or stretched exponential function, $q(t) = q_0 \exp[-(t/\tau)^\beta]$, where τ is the relaxation time, and β is called the nonexponential factor. $\beta = 1$ corresponds to an exponential, Arrhenius-like relaxation.[18] The temperature

dependence of τ can be fitted by the Vogel-Tamman-Fulcher (VTF) function, $\tau(T) = \frac{1}{f_l} \exp[\frac{W}{k_B(T_0 - T)}]$, where f_l is the libron frequency.[45,46] When $T_0 = 0$ K, the Arrhenius equation is realized and W corresponds to the activation energy. According to empirical observations, T_0 corresponds to the temperature of an ideal glass state ("Kauzmann temperature"), at which the crystal and the extrapolated glass state attain equal entropies[46] and the relaxation time becomes infinite.

Both β and $\frac{T_0}{T_g}$ are a measure of the deviation from Arrhenius relaxation. The relaxation in solid C_{60} was found to differ slightly from a purely exponential decay ($\beta = 0.94$).[18] The kinetic behavior of the C_{60} monolayer grown on the WO_2/W(110) surface is influenced by several factors. The low-temperature glassy state of the C_{60} film is characterized by a random orientation of the molecules [Fig. 1(a)]. In contrast, the glassy state in solid C_{60} is characterized by the random freezing of molecules among just two states. The large number of different molecular orientations observed in the film results in an averaging-out of the interaction potentials and should cause Arrhenius-like relaxation processes. However, STM experiments reveal correlations in the nanomotion of the C_{60} molecules that suggest arguments in favor of a constrain-dynamic scenario.[47] We suggest that the mechanism for the molecule-molecule interaction required for such a constrain-dynamic scenario can be based on some molecules acquiring charge. Indeed, our time-resolved STM experiments demonstrate that the rotational transition of an individual C_{60} molecule between states is accompanied by charge transfer to the molecule,[48] and subsequently, charge carried by a molecule affects the energy levels and barrier heights of its neighboring molecules via the Coulomb interaction.

From the lifetime of a molecule at a single state, we have found the potential barrier height separating the states to be 617 meV. If one assumes that the bulk libron frequency of $f_l = 10^{12}$ Hz and the relaxation time at the temperature of glassy transition for solid C_{60}, $\tau_S(90\text{K}) = 1$ day, can be applied to the film, then the VTF law can be used to estimate the Kauzmann temperature T_0. The obtained value $T_0 = 45$ K indicates that the relaxation process in the C_{60} monolayer film is close to the Arrhenius scenario of $\frac{T_0}{T_g} = 0.2$.

In summary, time-resolved STM investigations of the C_{60} monolayer deposited on the WO_2/W(110) surface reveal a rotational phase transition at 259 K and a kinetic glassy transition at 220 K. The temperature of the rotational phase transition is identical to that of 3D C_{60} crystals (259 K) and the temperature of the kinetic transition is substantially higher (220 K) than the bulk (90 K). Different mechanisms of molecular nanomotion, such as rotation, spinning, and switching between different orientations, have been observed. The total energy of the molecular interaction in the film is 48 meV, as estimated from mean-field theory. This was found to be approximately a factor of two greater than the energy level separation of an individual C_{60} molecule, as determined from time-resolved STM experiments.

The measurements of the phase transition temperature T_C in the film, combined with the argument for the reduced coordination number, suggests a strong contribution from the interaction between the molecules and the substrate. The energy of such interactions was estimated to be 24 meV. The observation of a glassy transition at 220 K reveals a non-exponential relaxation in the C_{60} monolayer. The Kauzmann temperature was estimated to be 45 K.

Our experiments have demonstrated the effectiveness of STM in the investigation of phase and kinetic transitions in the vicinity of critical temperatures. This is an unexpected result because, in general, the characteristic times of molecular and atomic motion are of the order of picoseconds and the characteristic frequency cutoff of an STM is much slower at 10 kHz ($\sim$100 μs). However, as the dynamics are highly temperature dependent, one can find a temperature range where the fluctuations happen on a time scale able to be resolved by STM and thus the temperature of the kinetic transition can be extracted.

ACKNOWLEDGMENTS

This work was supported by Science Foundation Ireland (Principal Investigator Grant No. 00/PI.1/C042 and Walton Visitor Award Grant No. 08/W.1/B2583) and by the Program of Presidium of the Russian Academy of Sciences.

*ivchvets@tcd.ie

[1] J. Zhao, K. Tatani, and Y. Ozaki, Appl. Spectrosc. **59**, 620 (2005).
[2] H. W. J. Blöte, W. Guo, and H. J. Hilhorst, Phys. Rev. Lett. **88**, 047203 (2002).
[3] O. Lübben, L. Dudy, A. Krapf, C. Janowitz, and R. Manzke, Phys. Rev. B **81**, 174112 (2010).
[4] H. Lüth, *Solid Surfaces, Interfaces and Thin Films* (Springer, 2001).
[5] I. Lyuksyutov, A. G. Naumovets, and V. Pokrovsky, *Two-Dimensional Crystals* (Naukova Dumka, 1988).
[6] P. M. P. Papon and J. Leblond, *The Physics of Phase Transitions: Concepts and Applications* (Springer, 2006).
[7] J. Kosterlitz and D. Thouless, J. Phys. C **6**, 1181 (1973).
[8] A. Hashimoto, *Handbook of Nanophysics: Nanoelectronics and Nanophotonics* (CRC Press, 2011), Chap. C_{60} Field Effect Transistors.
[9] D. M. Guldi, B. M. Illescas, C. M. Atienza, M. Wielopolski, and N. Martin, Chem. Soc. Rev. **38**, 1587 (2009).
[10] H. Park, J. L. Park, K. L. Andrew, E. H. Anderson, A. P. Alivisatos, and P. L. McEuen, Nature (London) **407**, 57 (2000).
[11] R. D. Johnson, C. S. Yannoni, H. C. Dorn, J. R. Salem, and D. S. Bethune, Science **255**, 1235 (1992).
[12] W. I. F. David, R. M. Ibberson, J. C. Matthewman, K. Prassides, T. J. S. Dennis, J. P. Hare, H. W. Kroto, R. Taylor, and D. R. M. Walton, Nature (London) **353**, 147 (1991).
[13] W. I. F. David, R. M. Ibberson, T. J. S. Dennis, J. P. Hare, and K. Prassides, Europhys. Lett. **18**, 219 (1992).
[14] R. Moret, Acta Crystallogr. Sect. A **61**, 62 (2005).
[15] S. L. Chaplot, L. Pintschovius, M. Haluska, and H. Kuzmany, Phys. Rev. B **51**, 17028 (1995).

[16]W. Schranz, A. Fuith, P. Dolinar, H. Warhanek, M. Haluska, and H. Kuzmany, Phys. Rev. Lett. **71**, 1561 (1993).
[17]F. Gugenberger, R. Heid, C. Meingast, P. Adelmann, M. Braun, H. Wühl, M. Haluska, and H. Kuzmany, Phys. Rev. Lett. **69**, 3774 (1992).
[18]F. Yan, Y. N. Wang, and J. S. Liu, Europhys. Lett. **48**, 662 (1999).
[19]J. P. Lu, X.-P. Li, and R. M. Martin, Phys. Rev. Lett. **68**, 1551 (1992).
[20]T. Matsuo, H. Suga, W. I. F. David, R. M. Ibberson, P. Bernier, A. Zahab, C. Fabre, A. Rassat, and A. Dworkin, Solid State Commun. **83**, 711 (1992).
[21]Y. Yoneda, K. Sakaue, and T. Terauchi, J. Phys. Condens. Matter **9**, 2851 (1997).
[22]D. Lamoen and K. H. Michel, J. Chem. Phys. **101**, 1435 (1994).
[23]D. Passerone and E. Tosatti, Surf. Rev. Lett. **4**, 859 (1997).
[24]C. Laforge, D. Passerone, A. B. Harris, P. Lambin, and E. Tosatti, Phys. Rev. Lett. **87**, 085503 (2001).
[25]A. N. Chaika, V. N. Semenov, V. G. Glebovskiy, and S. I. Bozhko, Appl. Phys. Lett. **95**, 173107 (2009).
[26]K. Radican, S. Bozhko, S.-R. Vadapoo, S. Ulucan, H.-C. Wu, A. McCoy, and I. Shvets, Surf. Sci. **604**, 1548 (2010).
[27]S. Krasnikov, S. Bozhko, K. Radican, O. Lübben, B. Murphy, S.-R. Vadapoo, H.-C. Wu, M. Abid, V. Semenov, and I. Shvets, Nano Research **4**, 194 (2011).
[28]X. Lu, M. Grobis, K. H. Khoo, S. G. Louie, and M. F. Crommie, Phys. Rev. B **70**, 115418 (2004).
[29]J. A. Larsson, S. D. Elliott, J. C. Greer, J. Repp, G. Meyer, and R. Allenspach, Phys. Rev. B **77**, 115434 (2008).
[30]G. Kresse and J. Furthmüller, Phys. Rev. B **54**, 11169 (1996).
[31]D. M. Ceperley and B. J. Alder, Phys. Rev. Lett. **45**, 566 (1980).
[32]S. B. Trickey, F. Müller-Plathe, G. H. F. Diercksen, and J. C. Boettger, Phys. Rev. B **45**, 4460 (1992).
[33]S. Saito and A. Oshiyama, Phys. Rev. Lett. **66**, 2637 (1991).
[34]S. Okada, S. Saito, and A. Oshiyama, Phys. Rev. Lett. **86**, 3835 (2001).
[35]J.-C. Charlier, X. Gonze, and J.-P. Michenaud, Europhys. Lett. **28**, 403 (1994).
[36]N. Troullier and J. L. Martins, Phys. Rev. B **46**, 1754 (1992).
[37]J.-C. Charlier, X. Gonze, and J.-P. Michenaud, Europhys. Lett. **29**, 43 (1995).
[38]L. A. Girifalco and M. Hodak, Phys. Rev. B **65**, 125404 (2002).
[39]M. Vanin, J. J. Mortensen, A. K. Kelkkanen, J. M. Garcia-Lastra, K. S. Thygesen, and K. W. Jacobsen, Phys. Rev. B **81**, 081408 (2010).
[40]M. Fujimoto, *The Physics of Structural Phase Transitions* (Springer, 2005), p. 39.
[41]S. Savin, A. B. Harris, and T. Yildirim, Phys. Rev. B **55**, 14182 (1997).
[42]F. Tournus, J.-C. Charlier, and P. Mèlinon, J. Chem. Phys. **122**, 094315 (2005).
[43]A. Goldoni, C. Cepek, R. Larciprete, L. Sangaletti, S. Pagliara, G. Paolucci, and M. Sancrotti, Phys. Rev. Lett. **88**, 196102 (2002).
[44]A. Glebov, V. Senz, J. P. Toennies, and G. Gensterblum, J. Appl. Phys. **82**, 2329 (1997).
[45]M. D. Ediger, C. A. Angell, and S. R. Nagel, J. Phys. Chem. **100**, 13200 (1996).
[46]F. H. Stillinger, Science **267**, 1935 (1995).
[47]R. G. Palmer, D. L. Stein, E. Abrahams, and P. W. Anderson, Phys. Rev. Lett. **53**, 958 (1984).
[48]S. Krasnikov, S. Bozhko, K. Radican, O. Lübben, B. Murphy, V. Semenov, H.-C. Wu, and I. Shvets, in 18th Interdisciplinary Surface Science Conference, Warwick University, UK, 2011, p. 13.